

Study of a near-threshold scalar resonance in the $\omega\phi$ system in pion-Be interaction at momentum of 29 GeV

V.A. Dorofeev¹, D.R. Ereemeev¹, V.G. Gotman¹, A.V. Ivashin¹, I.A. Kachaev¹, Yu.A. Khokhlov^{1,2*}, M.S. Kholodenko¹, V.F. Konstantinov^{1†}, V.I. Lisin¹, V.D. Matveev¹, E.V. Nazarov¹, V.I. Nikolaenko¹, A.N. Plekhanov¹, D.I. Ryabchikov¹, A.A. Shumakov¹, V.P. Sugonyaev¹ and A.M. Zaitsev^{1,2}

¹ NRC "Kurchatov Institute"- IHEP, Nauki Sq. 1, Protvino, 142281, Moscow region, Russia.

²MIPT, Institutsky Lane 9, Dolgoprudny, 141701, Moscow region, Russia.

*Corresponding author(s). E-mail(s): Yury.Khokhlov@ihep.ru;

†Deceased

Abstract

The charge-exchange reaction $\pi^- \text{Be} \rightarrow A \omega(782)\phi(1020)$ with $\omega \rightarrow \pi^+\pi^-\pi^0$ and $\phi \rightarrow K^+K^-$ is studied with the upgraded VES facility (U-70, Protvino) using a 29 GeV pion beam. The distribution of the $\omega\phi$ invariant mass shows a near-threshold enhancement. Partial-wave analysis reveals that an isoscalar scalar state with $J^{PC} = 0^{++}$ dominates in this mass region. Considering the observed signal as an f_0 resonance, and using the one-pion-exchange model, the product of the branching fractions into two channels $Br(f_0 \rightarrow \pi\pi)Br(f_0 \rightarrow \omega\phi)$ is measured. Based on this value, a large partial width is found for the radiative decay of J/ψ into this state, which suggests a significant glueball component. The result is discussed under alternative assumptions concerning an identification of the observed signal as $f_0(1710)$ or $f_0(1770)$.

Keywords: VES Experiment, IHEP Protvino, fixed target, charge exchange reaction, OPE, partial-wave analysis, scalar resonance, OZI rule, ω , ϕ , $f_0(1710)$, $f_0(1770)$, glueball

1 Introduction

The sector of scalar mesons holds a unique position in light-meson spectroscopy due to the uncertainty and redundancy in assigning the observed states to the quark-model $SU(3)_{\text{flavor}}$ nonets.

Resonance structures with quantum numbers $I^G J^{PC} = 0^+ 0^{++}$ are observed in several reactions in the mass range from 1700 to 1800 MeV. The Particle Data Group (PDG) [1] combines most of these observations into a single and established resonance, known as the $f_0(1710)$, with parameters

$$M = 1733_{-7}^{+8} \text{ MeV}, \quad \Gamma = 150_{-10}^{+12} \text{ MeV} \quad . \quad (1)$$

Ref. [1] also contains a review of the experimental data and their interpretations.

The $f_0(1710)$ has been extensively studied in J/ψ radiative decays, with peaks observed in the 4π [2], $K\bar{K}$ [3, 4], $\pi\pi$ [5], and $\omega\phi$ [6, 7] channels. The $\omega\omega$ channel also shows a $0^+ 0^{++}$ state in this mass region [8], which can be associated with the $f_0(1710)$ as well. The partial width

$$Br(J/\psi \rightarrow \gamma f_0(1710) \rightarrow_{(4\pi, K\bar{K}, \pi\pi, \omega\phi, \omega\omega)})$$

is significantly larger than the partial widths for the J/ψ radiative decays to other scalars. This observation suggests that the $f_0(1710)$ may have a glueball nature [9].

Convincing evidence for two f_0 resonances with significantly different masses and branching fractions to major channels in the 1.7 to 1.8 GeV mass region are presented in Refs. [10, 11]. The parameters of these resonances were determined through a coupled-channel analysis of BESIII data in Ref. [12].

Our particular interest concerns the $\omega\phi$ channel. The BESII experiment reported in Ref. [6] a near-threshold peak with $J^{PC} = 0^{++}$ in the $\omega\phi$ invariant mass spectrum in the reaction $e^+e^- \rightarrow J/\psi \rightarrow \gamma\omega\phi$, which was later confirmed by BESIII in Ref. [7]. The VES experiment observed a similar signal in the interaction of a pion beam with a beryllium target [13].

The results presented in this paper are based on new data obtained with the upgraded VES setup and supersede the results of Ref. [13]. Our analysis employs the same partial-wave analysis technique as the preceding analysis, but uses an improved experimental setup with upgraded detectors, more detailed and accurate detector simulation, and more precise data. Additionally, we performed a cross-section measurement. This enables us to compare our result to data from J/ψ radiative decays and theoretical models.

This paper has the following structure: in Sec. 2, we give a description of the detector. Sections 3 and 4 describe the selection procedure and some general features of the reaction under study. In Sec. 5, we present the partial-wave analysis (PWA) of the $\omega\phi$ system. The results of the PWA are discussed in Sec. 6. The signal observed at the threshold in the scalar wave of the $\omega\phi$ system is similar to the signal in J/ψ radiative decay. To compare this signal in the two production reactions, we estimated the ratio of the scalar-wave intensities from our analysis and a previous VES analysis of the $\omega\omega$ channel [13, 14]. The ratio we find is consistent with the ratio observed in J/ψ decays. Therefore, we conclude that the object observed in the charge-exchange reaction is the same as the one observed in J/ψ radiative decays, which is assigned to the $f_0(1710)$ by the PDG. Applying the one-pion-exchange approximation to our data, we estimate the product of the branching fractions into $\pi\pi$ and $\omega\phi$ for the studied f_0 state. In the discussion of our result, we use two alternative assumptions: we identify the f_0 either with the $f_0(1710)$ with parameters given in Eq. (1), or with the $f_0(1770)$ from Ref. [12] with parameters

$$M = (1765 \pm 15) \text{ MeV}, \quad \Gamma = (180 \pm 20) \text{ MeV} \quad . \quad (2)$$

For both cases, we calculate the branching fraction for $J/\psi \rightarrow \gamma f_0$ and compare it with theoretical estimates for the radiative J/ψ decay to a glueball. Our findings are summarised in Sec. 7.

2 VES Setup

The VES fixed-target experiment is a wide-aperture magnetic spectrometer with electromagnetic calorimetry and particle identification (see Fig. 1). The setup has been in operation since 1988 [15] and is located at a secondary beam line of the U-70 proton synchrotron in Protvino. About a decade ago, the facility was significantly upgraded, while retaining the general structure. The electromagnetic calorimeter and a major part of the tracking detectors were replaced. The particle identification was improved. The setup was equipped with a new data acquisition and trigger system. These upgrades help to suppress backgrounds, increase the rate of data collection, extend the list of measurable reactions, and allow us to measure their cross sections.

The data used in this analysis were obtained with a nominal beam momentum of 29 GeV and a typical momentum spread of $\pm 1\%$. The intensity of the negatively charged particles delivered to the experiment was typically $(1 \text{ to } 2) \cdot 10^6/\text{s}$. The beam was composed of approximately 98.0% π^- , 1.6% K^- , and 0.2% \bar{p} . The remaining 0.2% were muons and electrons.

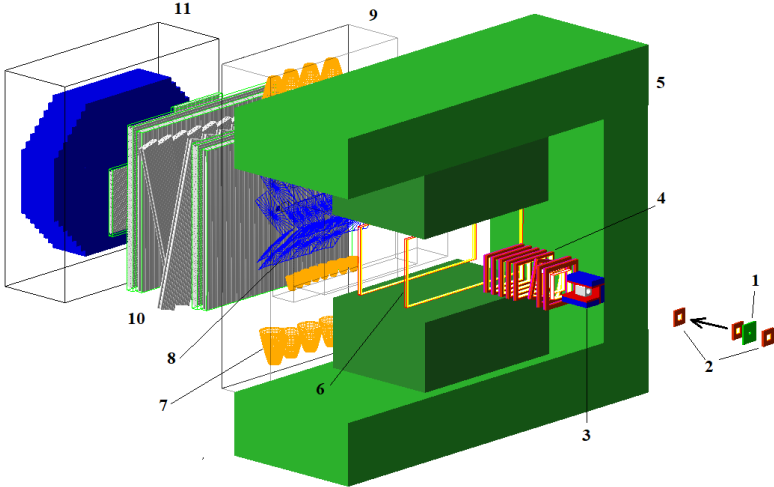


Fig. 1 Schematic view of the VES setup with the downstream counter of the beam telescope (1); the beam proportional chambers (2); the veto box with the target (3); the proportional chambers of the spectrometer (4); the spectrometer magnet (5); the drift chambers (6); the light-collecting cones (7), the mirrors (8), and the body (9) of the Cherenkov counter; the drift-tube stations (10); and the electromagnetic calorimeter (11). The arrow indicates the direction of the beam.

The beam section of the experiment (not shown in Fig. 1) consists of Cherenkov threshold counters for the identification of incoming pions, kaons, and antiprotons, beam-defining scintillators, and proportional chambers, which are used mainly for the beam particle tracking. Together with the last dipole magnet of the beam line they are also used to measure the beam momentum P_{beam} . The 1% accuracy of this measurement gives us limited control over nucleon excitations in the target-fragmentation kinematic region using the missing-mass technique.

The beryllium target has a diameter of 45 mm, which matches the beam spot size, and a thickness of 40 mm, which corresponds to about 10% of radiation and nuclear interaction lengths. The target is inserted into a hole in an aluminum holder (Fig. 2). The holder is a square prism of dimensions $12 \times 12 \times 20 \text{ cm}^3$. It absorbs slow recoiling protons and delta electrons. The hole in the holder has a cylindrical shape on the upstream side and a conical shape on the downstream side.

The target holder is surrounded on four sides by two layers of veto detectors, as shown in Fig. 3. The inner layer is composed of plastic scintillators, while the outer layer is made of Pb-scintillator sandwich detectors. The veto box is completed by two forward sandwich counters and a lead converter. The veto box rejects events where the produced particles leave the target at large angles. The trigger uses the scintillation-counter signals, while the signals from the sandwich detectors are digitized for offline analysis.

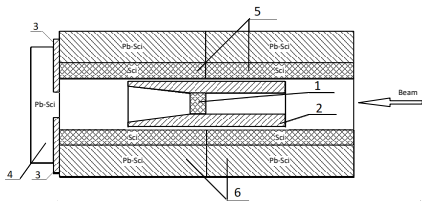


Fig. 2 Side view of the target region (not to scale), with the target (1); the holder (2); the lead converter (3); the forward sandwich detectors (4); the side scintillators (5), and the side sandwich detectors (6).

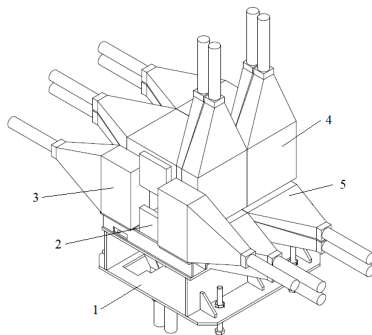


Fig. 3 The veto box surrounding the target, which includes the support (1), lead converters (2), forward sandwich detectors (3), side sandwich detectors (4), and side scintillators (5).

The veto box with the target is installed upstream of the main spectrometer magnet. This dipole magnet has an aperture that is about 2 m wide and 1 m high. The conical hole of the target holder and the veto counters match this aperture. At a current of 4 kA, the integral of the vertical field component is approximately 1.5 Tm.

Two 70 mm diameter scintillation disks, known as "Beam Killers" BK1 and BK2, are positioned downstream of the magnet along the nominal beam trajectory to suppress events without beam interaction.

The spectrometer's tracking system comprises proportional and drift chambers. Specifically, there are three two-plane multi-wire proportional chambers (MWPC) with an active area of approximately $40 \times 25 \text{ cm}^2$ and five two-plane MWPCs with a $60 \times 40 \text{ cm}^2$ active area at the entrance of the magnet. There are also two two-plane small-gap drift chambers inside the magnet and six planes of drift-tube detectors downstream of the magnet. Each drift-tube detector has dimensions of about $1.5 \times 2.0 \text{ m}^2$ and consists of three layers of 30 mm diameter drift tubes. The momentum resolution of the spectrometer is about 0.5% at 3 GeV and 1.2% at 25 GeV.

A 28-channel Cherenkov counter (Ch-28) is used to identify charged final-state particles. The threshold momentum for pions is about 3.5 GeV (see Ref. [16] for details).

The amount of material, that final-state photons have to traverse before reaching the electromagnetic calorimeter (EMC) [17] at the downstream end of the setup is less than 15% of radiation length. The parametrization of the energy resolution of the EMC is expressed as a quadratic sum: $\sigma_E/E = 0.069/\sqrt{E/1 \text{ GeV}} \oplus 0.027$ and is used in the 1C fit to the π^0 mass (see Sec. 3). The spatial resolution of EMC in the central part is 3.2 mm at 5 GeV.

Other systems of the upgraded setup are described in Refs. [18, 19].

3 Event selection

The analysis is based on data collected during four run periods between 2013 and 2015. About $2.3 \cdot 10^{11}$ beam particles passed through the beam telescope during the live time of the experiment. Events for the reaction

$$\pi^- \text{Be} \rightarrow \text{A } \omega(782)\phi(1020) \quad (3)$$

with $\omega \rightarrow \pi^+\pi^-\pi^0$ and $\phi \rightarrow K^+K^-$ are selected. Here, symbol A represents a final-state nucleus plus a recoil neutron that either remains in the nucleus or leaves it.

The event candidates for the exclusive event meson system are required to have four particle tracks, two with positive and two with negative charge, and two or three photon clusters in the EMC with energies $E_\gamma > 200$ MeV. If the third cluster, which is likely caused by noise in the EMC, is present, it should not be used in a π^0 candidate (see below) and its energy must not exceed 500 MeV. Noise clusters are γ -like signals in the EMC that are not related to a beam-induced reaction. They may be caused by δ electrons, pile-up hits, or electronic noise.

The distribution of the two-photon invariant mass $M_{\gamma\gamma}$ (Fig. 4) exhibits a Gaussian peak from $\pi^0 \rightarrow \gamma\gamma$, which has a width (RMS) of 6.0 MeV and a peak position that deviates by about 1 MeV from the nominal π^0 mass M_{π^0} . We select photon pairs with $|M_{\gamma\gamma} - M_{\pi^0}| < 20$ MeV as π^0 candidates.

To select events where the beam π^- interacted with the Be target, the position of the reconstructed interaction vertex is required to be within the target volume. The vertex reconstruction provides a spatial resolution of about 10 mm along the beam direction and of about 1 mm in the perpendicular plane.

In the momentum balance of the reaction, the recoil or potential target fragments can be omitted as the absolute value of the squared four-momentum t transferred from the beam to the target is small (see below). Hence, the closeness of the total momentum P_{tot} of the detected forward-going particles to P_{beam} is a measure for the exclusivity. The prominent peak in the P_{tot} distribution (see Fig. 15 and Sec. 4) is selected to impose exclusivity, i.e.

$$27.5 \text{ GeV} < P_{\text{tot}} < 31.0 \text{ GeV} \quad (4)$$

is required. The tail at low P_{tot} values indicates background from non-exclusive events.

Some events contain non-reconstructed large-angle tracks. These tracks appear as peripheral hits in the proportional chambers just after the target box. To enhance the exclusivity of the sample, events with short tracks are rejected.

Events where charged particles traverse either BK1 or BK2 are rejected at trigger level. In addition, none of the reconstructed tracks should pass through the circular regions, which are centred at the nominal positions of BK1 and BK2 and have a larger diameter of 80 mm. This takes into account

potential counter inefficiencies, uncertainties in their positioning, and tracking resolution.

The Ch-28 detector is used in the threshold regime to identify charged particles. Selected events have to have a higher likelihood for the $K^+K^-\pi^+\pi^-$ hypothesis than for the $4\pi^\pm$ hypothesis. Specifically, we limit the likelihood ratio to $\mathcal{L}(2K2\pi)/\mathcal{L}(4\pi) > \alpha_0$. The parameter α_0 controls both the efficiency and purity of the particle identification. We have chosen a value of $\alpha_0 = 2$ as a compromise between enhancing the ϕ signal discrimination and maintaining event statistics.

The invariant mass spectra for K^+K^- and $\pi^+\pi^-\pi^0$ in Figs. 5 and 6 show clear Gaussian-like peaks for $\phi(1020)$ and $\omega(782)$ within 2 MeV of their nominal masses [1], respectively. Both peaks sit on a substantial background. We constrain the energies of the two γ to the nominal π^0 mass in a 1C kinematic fit, resulting in a decrease of the Gaussian width of the ω peak from about 13 to 10 MeV.

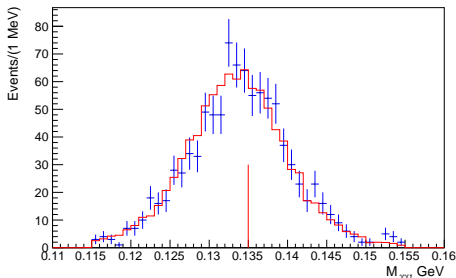


Fig. 4 The $M_{\gamma\gamma}$ invariant mass spectra for the selected measured events (in blue) and for the simulated data generated using the PWA result (in red). The nominal π^0 mass is indicated by the vertical line.

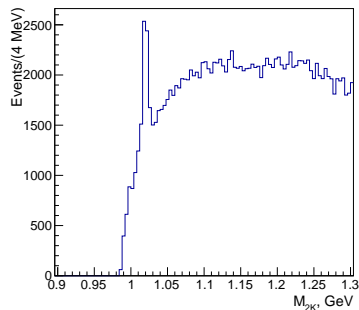


Fig. 5 K^+K^- invariant mass spectrum.

Figure 7 shows the two-dimensional distribution of the $\pi^+\pi^-\pi^0$ and the K^+K^- mass, with a clear signal for the associated production of ω and ϕ and less background than in the one-dimensional projections shown in Figs. 5 and 6.

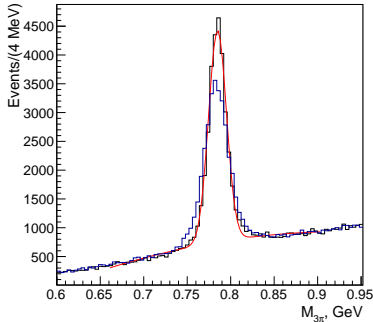


Fig. 6 The invariant mass spectrum of $\pi^+\pi^-\pi^0$ is shown in the black and blue histograms, with and without the 1C fit to the nominal mass of π^0 , respectively. The red curve represents a fit with a sum of a Gaussian and a quadratic function for signal and background, respectively.

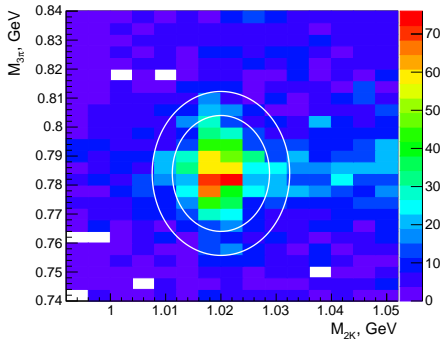


Fig. 7 Two-dimensional distribution of the invariant masses for $\pi^+\pi^-\pi^0$ and K^+K^- . The inner ellipse represents the signal region, while the elliptical ring corresponds to the background region.

The required signal events for reaction (3) have to lie within an ellipse in the $(M_{2K}, M_{3\pi})$ plane. This ellipse is defined by

$$r_{2M}^2 = \frac{(M_{3\pi} - M_\omega)^2}{\sigma_\omega^2} + \frac{(M_{2K} - M_\phi)^2}{\sigma_\phi^2} \leq 4. \quad (5)$$

Here, M_ω and M_ϕ are the nominal masses of $\omega(782)$ and $\phi(1020)$, respectively, taken from Ref. [1], and $\sigma_\phi = 4.4 \text{ MeV}$ and $\sigma_\omega = 10 \text{ MeV}$ are the RMS values for the corresponding Gaussian peaks. The selected region contains 1054 events.

4 General features of the $\omega\phi$ system

The M_{2K} and $M_{3\pi}$ spectra for the selected events in the signal region defined by Eq. (5) are shown in Figs. 8 and 9, respectively. For comparison, we superimpose the distributions for simulated data generated using the PWA result (see Sec. 5).

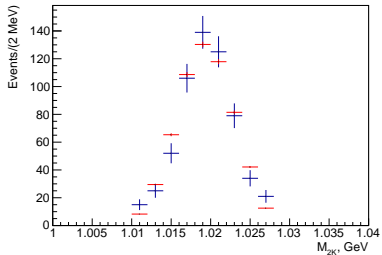


Fig. 8 K^+K^- invariant mass spectrum for the selected measured events (blue) and for simulated data generated using the PWA result (red).

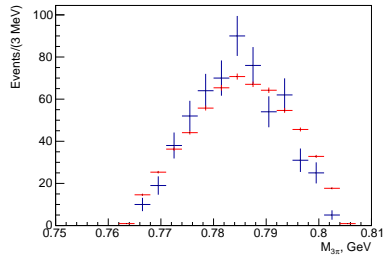


Fig. 9 $\pi^+\pi^-\pi^0$ invariant mass spectrum for the selected measured events (blue) and for simulated data generated using the PWA result (red).

The $\omega \rightarrow 3\pi$ decay is characterized by a linearly increasing distribution of events in the kinematic variable

$$\lambda = \frac{|\vec{p}_{\pi^-} \times \vec{p}_{\pi^+}|^2}{\lambda_{\max}}, \quad (6)$$

where $\lambda_{\max} = Q^2(Q^2/108 + m_\pi Q/9 + m_\pi^2/3)$ and $Q = T_{\pi^+} + T_{\pi^-} + T_{\pi^0}$, with pion momenta \vec{p}_π and kinetic energies T_π in the 3π center-of-mass system (c.m.s.). The distribution of the experimental events is shown in Fig. 10. The constant component is mainly due to the non- ω background. Its contribution is estimated from a linear fit to be about 20%.

The spectrum of the $K^+K^-\pi^+\pi^-\pi^0$ invariant mass $M_{\omega\phi}$ is sharply peaked near the threshold (blue histogram in Fig. 11). This peculiarity is the main focus of our study. In contrast, the $M_{\omega\phi}$ spectrum in the elliptical region $4 < r_{2M}^2 \leq 8$, which contains mostly background (see Fig. 7), does not show this structure (red histogram in Fig. 11).

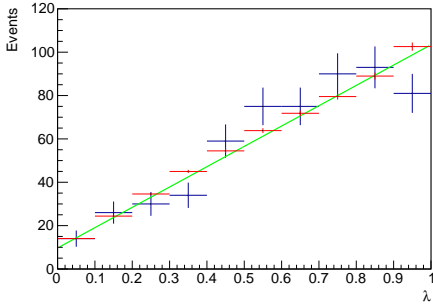


Fig. 10 Distribution of the kinematical variable λ in Eq. (6) for the selected measured events (blue) and for simulated data generated using the PWA result (red). The green line represents a linear fit to the experimental data.

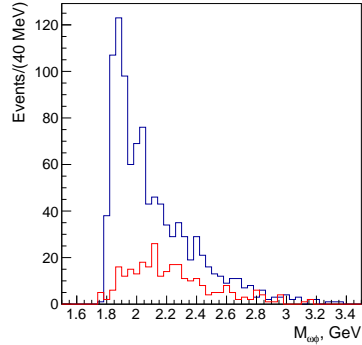


Fig. 11 $K^+K^-\pi^+\pi^-\pi^0$ invariant mass spectra in the signal region $r_{2M}^2 \leq 4$ (blue) and in the background region $4 < r_{2M}^2 \leq 8$ (red).

The distribution of the cosine of the Gottfried-Jackson angle of the ω momentum in the $\omega\phi$ rest frame is shown in Fig. 12. Its shape is strongly affected by the efficiency. In contrast, Fig. 13 shows the distribution of the cosine of the angle α between the normal of the ω decay plane in its c.m.s. and the K^+ momentum in the ϕ c.m.s., which is less affected by the efficiency. This distribution has a distinct parabolic-like component $\propto \cos^2\alpha$, as expected for the decay of a spinless particle to two vector particles with an orbital angular momentum of $L = 0$. Therefore, this distribution indicates a significant contribution from a $J^{PC} = 0^{++}$ state.

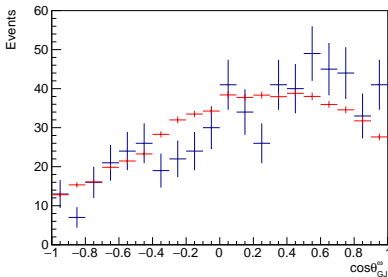


Fig. 12 Distribution of the cosine of the Gottfried-Jackson angle of the ω momentum in the $\omega\phi$ rest frame for the selected measured events (in blue) and for simulated data generated using the PWA result (in red).

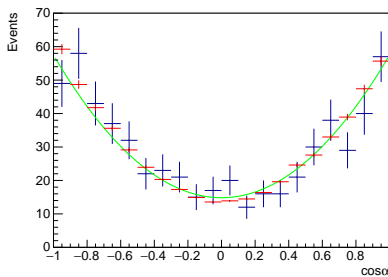


Fig. 13 Distribution of the cosine of the angle α between the normal of the ω decay plane in its rest frame and the K^+ momentum in the ϕ rest frame for the selected measured events (in blue) and for simulated data generated using the PWA result (in red). The green curve represents a quadratic function fitted to the experimental data.

The elliptical cut described in Eq. (5) results in some background being present below the two-dimensional $\omega\phi$ peak. In the partial-wave analysis outlined in Sec. 5, this background is not subtracted but is instead effectively accounted for in the PWA model. In this section, we present kinematic distributions where we subtracted this background. The non- ω background is removed through bin-by-bin subtraction applied to the sample without the cut in Eq. (5). For each bin of the variable in question, we require M_{2K} to lie within the ϕ band and fit the uncut $M_{3\pi}$ distribution with the sum of a linear background and a Gaussian signal. In this fit, the Gaussian parameters are fixed to the M_ω and σ_ω values from Eq. (5). The number of signal events, N_ω , fitted and plotted as a function of the binned variable value, corresponds to the background-subtracted distribution.

The background-subtracted t' spectrum is shown in Fig. 14, where $t' = |t| - |t|_{\min}$.¹ Since $|t|_{\min}$ is small, the difference between t' and $|t|$ can be ignored in our kinematics. We will use t in the following sections. The momentum transfer is calculated using the momenta of the beam and the reaction products in the forward region, so that nuclear effects including Fermi motion do not influence this measurement. The uncertainty in $|t|$, determined by a typical resolution of 8 MeV on the transverse momentum with respect to the beam, is $\sigma_{|t|} \approx 0.006 \text{ GeV}^2$ for $|t| = 0.15 \text{ GeV}^2$.

The neutral $\omega\phi$ system under study has positive G -parity and can be produced via one-pion exchange (OPE). Fitting the t distribution with the shape

$$\frac{dN_\omega}{dt} \propto \frac{t e^{\beta t}}{(t - m_\pi^2)^2} \quad (7)$$

yields a slope of $\beta = (4.3 \pm 0.5) \text{ GeV}^{-2}$. However, the fit quality is poor with $\chi^2/n.d.f = 36/11$.

The slopes in the OPE parametrization, obtained in Ref. [20] for pion-induced production of $\rho(770)$, $f_2(1270)$, and $\rho_3(1690)$ mesons at 17.2 GeV beam momentum, range from 7.0 to 8.2 GeV^{-2} . The energy dependence of the slope for the f_2 can be found in Ref. [21]. From this, we can evaluate the slope for $q\bar{q}$ resonances such as ρ , f_2 , and ρ_3 to be approximately $\beta \approx (8.2 \pm 0.2) \text{ GeV}^{-2}$. This value differs from the slope we obtained for the $\omega\phi$ data. The cause is unknown and requires further study.

The P_{tot} spectrum after background subtraction, without the exclusivity cut described in Eq. (4), is presented in Fig. 15 and was previously discussed in Sec. 3.

¹Here, $|t|_{\min}$ is the minimum value of $|t|$.

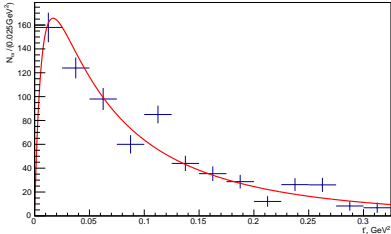


Fig. 14 t' spectrum with non- ω background subtracted is presented (histogram with error bars). The solid curve represents the fit with the OPE model in Eq. (7).

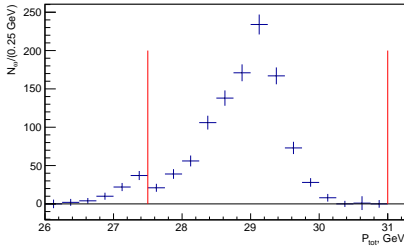


Fig. 15 P_{tot} spectrum with the non- ω background subtracted. The red lines indicate the applied exclusivity cut.

The background subtraction of the distributions discussed above was also performed by fitting the ϕ peak in the M_{2K} distribution while requiring $M_{3\pi}$ to be within the ω band. The results obtained are compatible with those shown above.

5 Partial-Wave Analysis

A mass-independent partial-wave analysis of the $\omega\phi$ system was performed in 60 MeV wide $M_{\omega\phi}$ bins ranging from 1.78 to 2.80 GeV. The $|t|$ range in the PWA was chosen from 0 to 0.15 GeV² (see also below) without binning, resulting in $N = 580$ events. The aim is to suppress possible contributions from production mechanisms other than OPE that have a wider t distribution.

In the PWA model, the decay of the produced intermediate states to $\omega\phi$ is approximated as a two-body decay. Symmetrization with respect to the final-state particles is not required, which distinguishes this analysis from the otherwise similar PWA of the $\omega\omega$ system in Ref. [14].

We use the extended maximum-likelihood method with the log-likelihood function

$$\log \mathcal{L} = \sum_{k=1}^N \log \sum_{\eta=\pm 1} \left| \sum_i T_i^\eta A_i^\eta(\tau_k) \right|^2 - \sum_{\eta=\pm 1} \sum_{i,j} T_i^\eta T_j^{\eta*} \int A_i^\eta(\tau) A_j^{\eta*}(\tau) \zeta(\tau) d\tau \quad , \quad (8)$$

which is defined such that the indices i and j enumerate the partial-wave amplitudes. For each value of i , the total amplitude is factorized into the unknown production amplitude T_i and the known decay amplitude A_i . To account for parity conservation at the $\omega\phi$ production vertex, the reflectivity basis [22] is used. In the high-energy limit, the reflectivity quantum numbers $\eta = +1$ and $\eta = -1$ correspond to natural and unnatural parity of the exchange particle, NPE and UPE, respectively (Refs. [23, 24]). The T_i^η are estimated by maximizing Eq. 8 for each $M_{\omega\phi}$ bin independently.

The custom PWA program calculates the first and second derivatives of $\log \mathcal{L}$ with respect to the fit parameters T_i^η analytically, resulting in faster fit convergence.

The decay amplitudes $A_i^\eta(\tau_k)$ are calculated for each event k with coordinates τ_k in the phase space. The construction of the decay amplitudes is based on Zemach's non-relativistic tensor formalism, as described in Ref. [25], which we extended to cover the case of two particles with non-zero spins. In our case, we first construct two tensors of rank $j = 1$: one from the K^+ three-momentum vector \vec{q}_1 in the ϕ c.m.s, and one from the normal \vec{q}_2 of the ω decay plane, which is given by the direction of $\vec{p}_{\pi^-} \times \vec{p}_{\pi^+}$ in the ω rest frame. Using these tensors, a rank- S tensor is constructed, where S is the total intrinsic spin of the $\omega\phi$ system. For $S = 2$, this tensor is symmetric and traceless. Next, we construct a rank- L tensor using the three-momentum of the ω in the $\omega\phi$ rest frame. Here, L represents the orbital angular momentum between ω and ϕ . Finally, we couple the L and S tensors to a tensor of rank J , where J is the spin of the intermediate state. This tensor is further projected according to the spin-projection quantum number $0 \leq M \leq J$ with respect to the beam direction in the Gottfried-Jackson frame of the $\omega\phi$ system. The wave notation is $J^{PC}M^\eta LS$. For instance, the decay amplitude for the wave $0^{++}0^-00$ has the structure $A \propto (\vec{q}_1 \cdot \vec{q}_2)$.

To account for the line shapes of ω and ϕ the decay amplitudes include square roots of corresponding Gaussian functions in $M_{3\pi}$ and M_{2K} , respectively. This helps to separate the non- ω and/or non- ϕ backgrounds from the signal process. To account for these backgrounds and imperfections of the PWA model, a so-called FLAT amplitude is added incoherently to the model in Eq. (8). This amplitude uniformly fills the $KK\pi\pi\pi$ phase space, i.e. $A_{\text{FLAT}} = \text{const}$.

The matrix of the normalisation integrals in the second term of Eq. (8) contains the acceptance function $\zeta(\tau)$. The decay amplitudes are normalised such that $\int |A_i^\eta|^2 d\tau = 1$. This gives acceptance-corrected wave intensities $I_i^\eta = |T_i^\eta|^2$, expressed in terms of the number of produced events, with relative phases $\phi_i^\eta - \phi_j^\eta = \arg(T_i^\eta T_j^{\eta*})$. The integrals are pre-calculated once before the fit procedure using the Monte Carlo (MC) technique. The MC simulation of the experimental setup and of the passage of particles through this setup is based on the Geant4 10.5 package [26]. The reconstruction and selection procedures applied to the simulated data are the same as for the real data. The performance of the experiment was generally the same over the four running periods used in this analysis, with minor differences in details, such as changes in the beam momentum within 0.5 GeV and in the position of detectors within 1 cm and others. Separate MC models were used for all significant time periods.

It was checked that both the general characteristics of the event samples and the results of the PWA for the different running periods were compatible. Then the PWA was performed on the combined data sample. For this PWA, we used the total MC sample, where the number of MC events generated for each run period is proportional to the number of events recorded in the

period divided by the corresponding efficiency. This means that we average the efficiency over the run periods with weights proportional to the number of events produced in each run period.

A small set of waves proved sufficient to describe the data well. These waves are: FLAT, $0^{++}0^{-}00$, $2^{++}0^{-}02$, $0^{-+}0^{+}11$. The intensity distributions of these waves obtained from the PWA fit are shown in Fig. 16. None of the waves can be excluded from the PWA fit without significantly degrading the quality of the fit. Other waves, when added, prove to be insignificant and do not improve the fit quality. This justifies our choice of the minimalist PWA model.

The intensities of the waves integrated over $M_{\omega\phi}$ relative to the integral of the total intensity are 58% for 0^{++} , 20% for 2^{++} , 9% for 0^{-+} , and 13% for FLAT. The scalar wave with $J^{PC} = 0^{++}$ is the dominant wave and has a peak at threshold. The tensor wave 2^{++} also shows some peak behaviour but it is much less pronounced. The other two waves are smaller and have no significant structures.

To check the stability of the analysis with respect to the chosen cut value α_0 for the PID likelihood ratio (see Sec. 3), the PWA was re-run with $\alpha_0 = 1$ and $\alpha_0 = 4$. The resulting partial-wave amplitudes remain stable within statistical uncertainties. In the absence of a MC model for the misidentified background, we take this as evidence for the smallness of this background.

To reveal the role of the non- $\omega\phi$ background, we performed the PWA with a looser elliptical cut in the $(M_{2K}, M_{3\pi})$ plane, i.e. using Eq. (5) with $\sigma_\phi = 8.8$ MeV and $\sigma_\omega = 22$ MeV. The only statistically significant change in the wave intensities is an increase of the FLAT wave, which is roughly proportional to the increase in elliptical area. This suggests that the non- $\omega\phi$ background dominates in the FLAT wave.

The UPE waves make up 78% of the total intensity of the process under study, which supports the hypothesis of the OPE production mechanism. An alternative PWA with a wider cut of $|t| < 0.5 \text{ GeV}^2$ is expected to have a smaller contribution from the UPE waves. The fit results in relative intensities of 56% for 0^{++} , 17% for 2^{++} , 8% for 0^{-+} , and 20% for FLAT waves. This indicates a decrease in the contribution of the UPE waves to 73%.

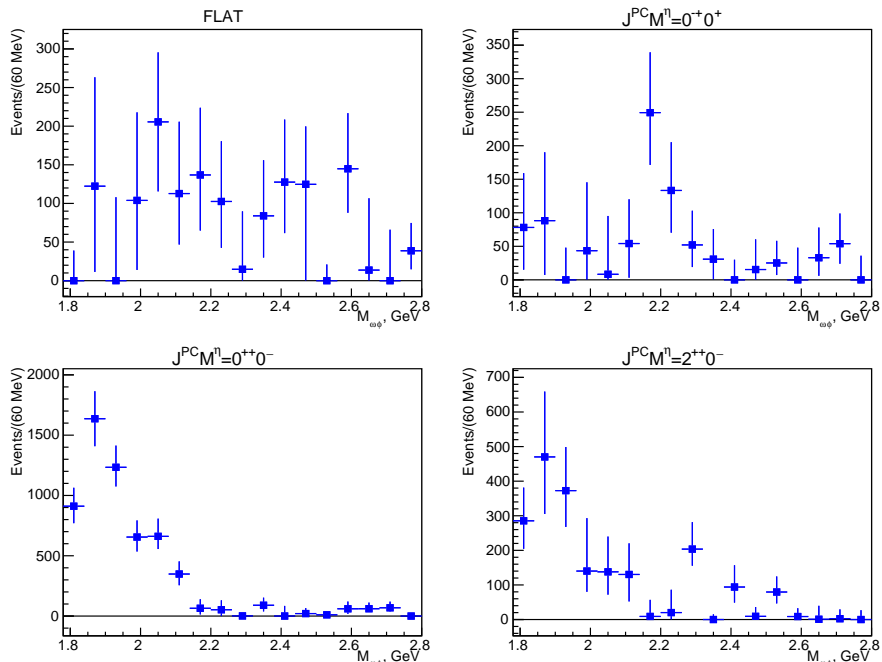


Fig. 16 Partial-wave intensities obtained from the final PWA result with $|t| < 0.15 \text{ GeV}^2$.

6 Results and Discussion

The wave intensities in the final PWA results for $|t| < 0.15 \text{ GeV}^2$ are presented in Fig. 16. Due to a positivity constraint and small sample size, evaluating errors of PWA results based on the inverse of the Hessian matrix of the log-likelihood function at its maximum can be biased. Instead, we evaluate intensity errors, represented as asymmetric bars, by scanning the log-likelihood value as a function of the intensity near its maximum and determining the intensity interval that corresponds to a decrease of the maximum log-likelihood by half a unit.

In this PWA, only the phase between the 0^{++} and the 2^{++} waves is available. However, in the case of narrow resonances the measurement of the phase is twofold ambiguous. Two solutions are shown in the Fig. 17 for a limited mass range. For higher masses, the phase cannot be measured due to the smallness of the intensities. There is no definitive interpretation for the phase motion in the 0^+ wave due to the ambiguity and the absence of a model for the reference 2^+ wave.

In the range of $M_{\omega\phi}$ shown, the total efficiency, including the cuts, varies slowly with the $M_{\omega\phi}$ between 5.1% and 6.7%. A comparison of the measured distributions with those obtained from the Monte Carlo events weighted with the PWA result is shown in Figs. 4,8,9,10,12 and 13. The model describes the

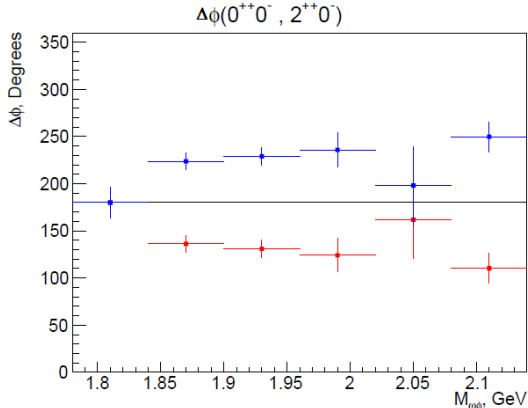


Fig. 17 Phase difference between the 0^{++} and the 2^{++} waves. Two solutions are shown with different colours. The horizontal line indicates 180 degrees.

experimental data rather well. The Monte Carlo events were generated using Breit-Wigner amplitudes for ω and ϕ , with their nominal masses and widths.

6.1 Comparison of $\omega\phi$ and $\omega\omega$ channels

In this section, we compare the characteristics of the reactions $\pi^- \text{Be} \rightarrow A\omega\phi$ and $\pi^- \text{Be} \rightarrow A\omega\omega$ with the predictions of the OZI rule [27–29]. The characteristics of these channels in charge-exchange reactions and in radiative J/ψ decays are also compared, and it is found that the same signal is observed.

To this end, we use the results of a PWA of the $\omega\omega$ system performed on data obtained with the VES setup at 28 GeV nominal beam momentum [13, 14]. In the following text, values from the $\omega\omega$ analysis are denoted by "28", while the values from our current analysis are denoted by "29". Here, these numbers indicate the slightly different beam momenta for the two data samples.

The data for $\omega\omega$ are dominated by $J^{PC} = 2^{++}$ waves across a broad mass range. The intensity $N_{\omega\omega,28}^{0^+}$ of the smaller $0^{++}0^-00$ $\omega\omega$ wave was extracted from Fig. 4 of Ref. [13], while the total intensity $N_{\omega\omega,28}$ was obtained by summing the UPE and NPE wave intensities (dashed histograms in Fig. 4 of Ref. [14]). The intensity of the 0^{++} wave is significant but lacks prominent structures. From these intensity distributions, we derive the relative contribution of the scalar wave, $N_{\omega\omega,28}^{0^+}/N_{\omega\omega,28}$, as a function of $M_{\omega\omega}$.

To establish a relationship between the 28-GeV and 29-GeV data samples, we need to know the $M_{\omega\omega}$ spectrum $N_{\omega\omega,29}^{\text{obs}}$ from the latter one. The selection requirements applied and the values for the cuts are in general similar to the $\omega\phi$ case. Characteristics specific to $\omega\omega$ are listed below. Particle identification is not applied to the four charged particles. Four to five photon clusters in the EMC are required. Two photons with an invariant mass within 25 MeV of the nominal π^0 mass are considered as neutral pions candidates. We construct all disjoint combinations of pairs of $\pi^+\pi^-\pi^0$ subsystems, where we allow for

one unassigned photon cluster. We select the pair with the smallest distance from the point that corresponds to nominal ω masses in the $(M_{3\pi}, M_{3\pi})$ plane within a circular region of 30 MeV radius about that point. Figure 18 shows the $M_{\omega\omega}$ spectrum after all selection cuts.

Next, the $N_{\omega\omega,29}^{\text{obs}}$ spectrum is corrected by the efficiency $\epsilon_{29}(M_{\omega\omega})$. It is estimated from a Monte Carlo simulation with the full chain of reconstruction and selection procedures. The event kinematics for the Monte Carlo is generated using the measured t distribution and the known distribution of λ for the two ω decays. The simulation of angular distributions is based on the dominant wave with $J = 2$ and $L = 0$. The value of ϵ_{29} is found to be weakly dependent on $M_{\omega\omega}$ in the analysed range, with an average value of $\langle\epsilon_{29}\rangle \approx 0.06$. To estimate the systematic uncertainty of the efficiency, Monte Carlo data were also generated for the $J = 0, L = 0$ wave. The efficiencies estimated using these data differ by typically 5% from the ones used in the main analysis.

With the above, the scalar wave intensity for the 29-GeV data is:

$$N_{\omega\omega,29}^{0+}(M_{\omega\omega}) = \frac{N_{\omega\omega,29}^{\text{obs}}}{\epsilon_{29}} \frac{N_{\omega\omega,28}^{0+}}{N_{\omega\omega,28}} C_t \quad . \quad (9)$$

To account for the wider range of $|t| < 0.20 \text{ GeV}^2$ used in the analysis of the 28-GeV data, an additional correction factor of $C_t = 1.13 \pm 0.03$ is applied.

Finally, in the mass region where both channels are open and in the range $|t| < 0.15 \text{ GeV}^2$, the ratio

$$R = \frac{N_{\omega\phi,29}^{0+}}{N_{\omega\omega,29}^{0+}} \frac{Br(\omega \rightarrow \pi^+\pi^-\pi^0)}{Br(\phi \rightarrow K^+K^-)} \quad (10)$$

of the $0^{++}0^-00$ wave intensities in the $\omega\phi$ and $\omega\omega$ decay channels is calculated. As shown in Fig. 19, R is close to 1. The error bars encompass the statistical and systematic uncertainties of all factors in Eqs. (9) and (10). The partial-wave intensities give the largest contribution.

We also calculate the ratio

$$R_A = R \frac{q_{\omega\omega}}{q_{\omega\phi}} \quad (11)$$

which is determined by the squared amplitudes of the two processes. Here, we account for the different phase-space by dividing the acceptance-corrected intensities by the corresponding breakup momenta $q_{\omega\omega}$ and $q_{\omega\phi}$ that are defined in the c.m.s. of the $\omega\omega$ and $\omega\phi$ system, respectively. The lowest mass bin is omitted due to the very rapid change of the breakup momentum near the threshold. Averaging the four bins in the mass range from 1.84 to 2.08 GeV yields a value of $\langle R_A \rangle(0^{++}) = 2.4 \pm 0.5$ with $\chi^2/\text{ndf} = 1.5/3$.

Applying the same procedure to the $2^{++}0^-02$ wave, we obtain R values, which are shown in Fig. 20. They results in $\langle R_A \rangle(2^{++}) = 0.30 \pm 0.08$ with $\chi^2/\text{ndf} = 2.3/3$.

The obtained $\langle R_A \rangle$ values can be compared to predictions based on the OZI rule [27–29]. For the interaction of particles composed of light quarks it states that the relative yield of the ϕ to ω mesons is determined by $\tan^2 \theta = 4.2 \cdot 10^{-3}$. Here the mixing angle $\theta = 3.7^\circ$ [30] is defined through the ϕ quark content: $\phi = s\bar{s} \cos \theta + n\bar{n} \sin \theta$. Experimental data on various reactions [30] indicate a significant suppression of reactions involving ϕ production, although this suppression is sometimes far less than the theoretical value.

The $\langle R_A \rangle (0^{++})$ value observed in our experiment did not show any suppression and is larger than that in all other experiments. The cause of this significant OZI rule violation is currently unknown. One possible explanation for this phenomenon is the substantial mixing of scalar states with different quark compositions. This mixing has been observed experimentally and can be explained by theoretical models [31]. In contrast, the mixing for the tensor states is much less [31], resulting in $\langle R_A \rangle (2^{++})$ value that is closer to the OZI prediction.

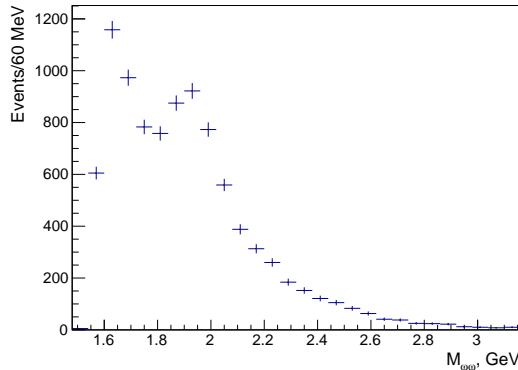


Fig. 18 The $\omega\omega$ invariant mass spectrum for the 29-GeV data sample.

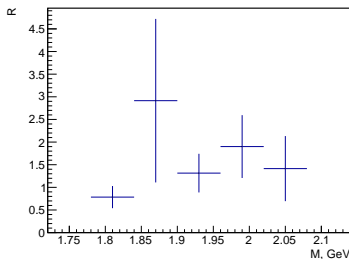


Fig. 19 Ratio of the $J^{PC} = 0^{++}$ wave intensities in the $\omega\phi$ and $\omega\omega$ channels as a function of mass (see Eq. (10)).

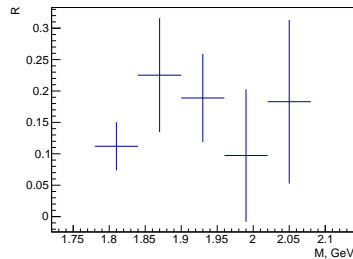


Fig. 20 Similar ratio as in Fig. 19 but for the $J^{PC} = 2^{++}$ wave.

The structure we observe in the scalar $\omega\phi$ wave is similar to the $X(1810)$ reported in radiative J/ψ decays to $\omega\phi$ in Refs. [6, 7]. These results are included by the PDG in the entry for the $f_0(1710)$ [1]. In order to verify that one and the same object is observed in the charge-exchange reaction and in the radiative J/ψ decays, we now compare the relative intensities of the production of the $J^{PC} = 0^{++}$ wave in the $\omega\omega$ and $\omega\phi$ channels in these two reactions.

From the PDG entry for the J/ψ we get

$$R_{\text{Rad.Dec.}} = \frac{Br(J/\psi \rightarrow \gamma f_0(1710) \rightarrow \gamma\omega\phi)}{Br(J/\psi \rightarrow \gamma f_0(1710) \rightarrow \gamma\omega\omega)} = 0.8 \pm 0.4 \quad . \quad (12)$$

The branching fraction for the $\omega\omega$ channel in Eq. (12) was measured for masses starting at the $\omega\omega$ threshold. For comparison, we now calculate the corresponding ratio for the charge-exchange reaction by summing the numerator and denominator in Eq. (10) over the mass bins from the $\omega\phi$ and $\omega\omega$ thresholds, respectively, up to 2.08 GeV. The extended mass range for the $\omega\omega$ channel leads to a lower value of $R_{\text{Ch.Ex.}} = 0.70 \pm 0.15$, compared to the values shown in Fig. 19. This value of $R_{\text{Ch.Ex.}}$ is consistent with $R_{\text{Rad.Dec.}}$.

Both the shape of the 0^{++} wave intensity in the $\omega\phi$ channel and its ratio to that in the $\omega\omega$ channel are consistent in radiative J/ψ decays and in charge-exchange reactions. This suggests that the same object is observed in both reactions.

6.2 Parameters of Scalar Resonance

We further consider two alternative assumptions regarding the identification of the observed signal. In the first assumption, the source of the signal is the $f_0(1710)$ from Ref. [1] with parameters given in Eq. (1), and in the second it is the $f_0(1770)$ from Ref. [12] with parameters given in Eq. (2).

Due to the proximity of the $f_0(1710)$ mass to the $\omega\phi$ threshold, we describe the wave intensity with a Flatté parameterisation, i.e.

$$\frac{dN}{dM} = \frac{CM_R^2\Gamma_0 gq_{\omega\phi}}{(M_R^2 - M^2)^2 + M_R^2(\Gamma_0 + gq_{\omega\phi})^2} \quad (M > M_\omega + M_\phi) \quad . \quad (13)$$

Here, Γ_0 is a constant partial width that accounts for the decay into channels that are far above their thresholds, and $gq_{\omega\phi}$ accounts for the mass-dependent partial width for the $\omega\phi$ channel. The shape of the curve is determined by three parameters: M_R , Γ_0 , and g , which are strongly correlated in the fit. However, when using Eq. 13 for numerical calculations, the branching fraction into the $\omega\phi$ channel closely approximates the value of g . This holds true regardless of the two other parameters that were reasonably chosen. To better constrain the model and stabilize the fit, we set the value of g to a middle value within the range of possible branching fractions. An upper limit for this range is

conservatively estimated using data from Ref. [1]. Specifically,

$$Br_{\max}(f_0(1710) \rightarrow \omega\phi) = \frac{\Gamma(J/\psi \rightarrow \gamma f_0(1710) \rightarrow \gamma\omega\phi)}{\Sigma\Gamma(J/\psi \rightarrow \gamma f_0(1710) \rightarrow \text{all observed channels})} = 0.14. \quad (14)$$

The minimum value of $Br_{\min}(f_0(1710) \rightarrow \omega\phi)$ is 0.05, as determined later in Eq. (20).

Fitting Eq. (13) to the 0^{++} wave intensity with a fixed value $g = 0.1$ yields resonance parameters of $M_R = (1834 \pm 14)$ MeV and $\Gamma_0 = (114 \pm 15)$ MeV, with a $\chi^2_{\min}/\text{ndf} = 13.3/5$ (see Fig. 21). Systematic uncertainties of the fit parameters were estimated by varying $g = 0.10 \pm 0.05$. So the resonance parameters of Eq. (13) are $M_R = (1834 \pm 14 (\text{stat.})_{-10}^{+2} (\text{syst.}))$ MeV and $\Gamma_0 = (114 \pm 15 (\text{stat.})_{-15}^{+5} (\text{syst.}))$ MeV. We verified that altering the range of the fitted mass does not affect the outcome.

The mass and width are compatible with the parameters of the $X(1810)$ reported in Ref. [7] for $J/\psi \rightarrow \gamma\omega\phi$ decay: $M = (1795 \pm 7_{-20}^{+23})$ MeV and $\Gamma = (95 \pm 10_{-82}^{+78})$ MeV .

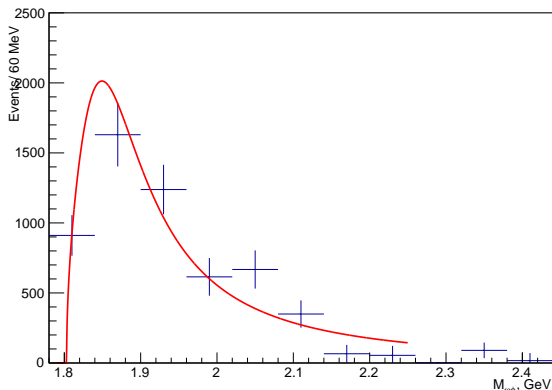


Fig. 21 The intensity of wave $0^{++}0^{-}00$ in the $\omega\phi$ channel (points from Fig. 16) fitted with the model function in Eq. (13) with $g = 0.1$.

6.3 Branching Fractions of Scalar Resonance

The intensity of the scalar wave integrated over the mass region $M_{\omega\phi} < 2.14$ GeV, where it is significant, amounts to $5.4 \cdot 10^3$ events. Accounting for the branching fractions for the ω and ϕ decays from PDG [1], this corresponds to a cross section of

$$\sigma(\pi^- \text{Be} \rightarrow \text{A} \omega\phi) (J^{PC} = 0^{++}, M_{\omega\phi} < 2.14 \text{ GeV}, |t| < 0.15 \text{ GeV}^2) = 98 \pm 7(\text{stat.}) \pm 7(\text{syst.}) \text{ nb} . \quad (15)$$

The systematic uncertainty is calculated as the quadratic sum of the uncertainties in the efficiency, cross-section normalization, and the two branching fractions.

We will use the cross section in Eq. (15) to evaluate the value of $Br(f_0 \rightarrow \pi\pi)Br(f_0 \rightarrow \omega\phi)$ using the one-pion-exchange model. To do this, we need to know the cross section for the charge-exchange reaction on the proton. Several theoretical and experimental works have related the cross sections of charge-exchange reactions on the proton to those on nuclei [32–34]. For light nuclei, the Z dependence of the cross section can be approximated by $\sigma \propto Z^\alpha$, where Z is the number of protons. Based on experimental data on the productions of isoscalars in charge-exchange reactions at a beam momentum of 39 GeV [34], we estimate that $\alpha = 0.73 \pm 0.03$. For Beryllium, this corresponds to $Z^\alpha = 2.7 \pm 0.2$. Using Eq. (15), we obtain

$$\sigma(\pi^- p \rightarrow n\omega\phi) (J^{PC} = 0^{++}, M_{\omega\phi} < 2.14 \text{ GeV}, |t| < 0.15 \text{ GeV}^2) = (36. \pm 5.) \text{ nb} \quad . \quad (16)$$

The systematic uncertainty dominates the total uncertainty. Here and below a PDG rounding rule is applied to numerical results.

We then proceed to calculate the product of $Br(f_0(1710) \rightarrow \pi\pi)$ and $Br(f_0(1710) \rightarrow \omega\phi)$ using the OPE approximation for the production of a resonance X decaying to a given channel [35, 36]:

$$\frac{d\sigma(\pi^- p \rightarrow nX)Br(X \rightarrow \text{channel})}{d|t|} = 26.9 \text{ mb } Br(X \rightarrow \pi\pi)Br(X \rightarrow \text{channel}) \frac{M_X \Gamma_X}{P_{\text{beam}}^2} \frac{|t| e^{\beta(t-m_\pi^2)}}{(t-m_\pi^2)^2} \quad . \quad (17)$$

This approximation is commonly used to analyse charge-exchange reactions with UPE dominance. The systematic uncertainty is estimated to be approximately 20% [20].

Integrating Eq. (17) over $|t|$ with $|t|_{\text{max}} = 0.15 \text{ GeV}^2$, $\beta = (4.3 \pm 0.5) \text{ GeV}^{-2}$ from Eq. (7), and $M_X \Gamma_X = (0.260 \pm 0.021) \text{ GeV}^2$ from Eq. (1), and using Eq. (16), we get

$$Br(f_0(1710) \rightarrow \pi\pi)Br(f_0(1710) \rightarrow \omega\phi) = (4.8 \pm 1.2) \cdot 10^{-3} \quad . \quad (18)$$

Using Ref. [1], we calculate the product

$$Br(J/\psi \rightarrow \gamma f_0(1710) \rightarrow \gamma\pi\pi)Br(J/\psi \rightarrow \gamma f_0(1710) \rightarrow \gamma\omega\phi) = (9.5 \pm 2.6) \cdot 10^{-8} \quad . \quad (19)$$

Using this value and Eq. (18), we find

$$Br(J/\psi \rightarrow \gamma f_0(1710)) = (4.5 \pm 0.8) \cdot 10^{-3} \quad . \quad (20)$$

If compared with the experimental value for the decay of the $f_0(1710)$ into the five channels $\pi\pi, KK, \eta\eta, \omega\omega$, and $\omega\phi$ listed by PDG [1]

$$Br(J/\psi \rightarrow \gamma f_0(1710))Br(f_0(1710) \rightarrow 5 \text{ channels}) = (2.13 \pm 0.18) \cdot 10^{-3}, \quad (21)$$

Eq. (20) leaves a branching fraction for unlisted channels of

$$Br(f_0(1710) \rightarrow 4\pi, 6\pi, \eta\eta', \pi\pi KK, \dots) = (2.3 \pm 0.8) \cdot 10^{-3}. \quad (22)$$

This value does not contradict the result of Ref. [2], i.e.

$$Br(f_0(1750) \rightarrow \sigma\sigma) = (9.0 \pm 1.3) \cdot 10^{-4}, \quad Br(f_0(1750) \rightarrow \rho\rho) = (1.90 \pm 0.14) \cdot 10^{-4}, \quad (23)$$

assuming that $f_0(1710)$ and $f_0(1750)$ are the same object.

Comparing the value obtained for $Br(J/\psi \rightarrow \gamma f_0(1710))$ in Eq. (20) with the value $(3.8 \pm 0.9) \cdot 10^{-3}$ calculated for a scalar glueball in Ref. [37] using quenched lattice QCD suggests the presence of a significant or even dominant glueball component in the $f_0(1710)$. This branching fraction is much lower for other known scalars [9].

To illustrate the properties of the $f_0(1710)$, we refer to the model presented in Ref. [38]. The model states that the branching of the radiative decay of a heavy vector quarkonium to a resonance R_J with spin J is proportional to the R_J decay width into two gluons. This can be expressed as

$$\frac{Br(Q\bar{Q}_V \rightarrow \gamma R_J)}{Br(Q\bar{Q}_V \rightarrow \gamma gg)} = K_J(M_R/M_V) \frac{M_R \Gamma_R Br(R_J \rightarrow gg)}{M_V^2}. \quad (24)$$

The function $K_J(M_R/M_V)$ contains a loop integral for virtual gluons in the $Q\bar{Q}_V \rightarrow \gamma R_J$ decay. This integral is calculated using a model for the form factor of R_J . Using the value $K_0(M_{f_0(1710)}/M_{J/\psi}) = 0.116$ from Ref. [38], the branching fraction $Br(J/\psi \rightarrow \gamma gg) = 0.088 \pm 0.011$ according to Ref. [1] and the branching fraction $Br(J/\psi \rightarrow \gamma f_0(1710))$ from Eq. (20), one can calculate the branching fraction for the $f_0(1710)$ decay to two gluons: $Br(f_0(1710) \rightarrow gg) = 1.7 \pm 0.4$. The quoted uncertainty is primarily due to the uncertainties of the J/ψ radiative-decay branching fractions and the OPE model. It does not include the systematics of the model from Ref. [38]. The measured branching fraction of about 1 indicates a significant glueball component in the $f_0(1710)$.

Ref. [12] provides strong evidence that the $f_0(1710)$ reported in Ref. [1] is actually split into two states, an $f_0(1710)$, which is distinct from the $f_0(1710)$ in the PDG, and an $f_0(1770)$. In the reaction $\pi^- p \rightarrow n\omega\phi$ we observe only one state, the $f_0(1770)$, while the other state, the $f_0(1710)$, does not contribute due to the smallness of its couplings to $\pi\pi$ and $\omega\phi$. The resonance parameters of the $f_0(1770)$ reported in Ref. [12] are:

- $M = (1765 \pm 15) \text{ MeV}, \quad \Gamma = (180 \pm 20) \text{ MeV},$
- $Br(J/\psi \rightarrow \gamma f_0(1770) \rightarrow \gamma\pi\pi) = (2.4 \pm 0.8) \cdot 10^{-3},$

- $Br(J/\psi \rightarrow \gamma f_0(1770) \rightarrow \gamma\omega\phi) = (2.2 \pm 0.4) \cdot 10^{-3}$.

Using these values in the above equations, we can determine the following values:

- $Br(f_0(1770) \rightarrow \pi\pi)Br(f_0(1770) \rightarrow \omega\phi) = (3.9 \pm 1.0) \cdot 10^{-3}$,
- $Br(J/\psi \rightarrow \gamma f_0(1770)) = (3.7 \pm 0.8) \cdot 10^{-3}$,
- $Br(f_0(1770) \rightarrow 4\pi, 6\pi, \eta\eta', \pi\pi KK\dots) = (1.6 \pm 0.9) \cdot 10^{-3}$,
- $Br(f_0(1770) \rightarrow gg) = 1.12 \pm 0.32$.

These values do not affect the conclusion regarding the significant presence of a glueball component in the studied f_0 state.

7 Conclusions

The reaction $\pi^-Be \rightarrow A\omega\phi$ was studied at a beam momentum of 29 GeV. The $J^{PC} = 0^{++}$ wave dominates in the $\omega\phi$ system and exhibits a threshold enhancement. The average ratio of the intensities of the 0^{++} wave in the $\omega\phi$ and $\omega\omega$ channels, corrected for phase space, was found to be $\langle R_A \rangle = 2.4 \pm 0.5$. This indicates a significant violation of the OZI rule.

We measure a cross section of

$$\sigma(\pi^-Be \rightarrow A\omega\phi) (J^{PC} = 0^{++}, M_{\omega\phi} < 2.14 \text{ GeV}, |t| < 0.15 \text{ GeV}^2) = 98 \pm 7(\text{stat.}) \pm 7(\text{syst.}) \text{ nb.}$$

The signal in the $\omega\phi$ channel can be attributed to the known $f_0(1710)$ from Ref. [1] or to the $f_0(1770)$ from Ref. [12]. Using the one-pion exchange model for the reaction $\pi^-p \rightarrow n f_0$ and the branching fractions for the radiative J/ψ decays, a branching fraction of $Br(J/\psi \rightarrow \gamma f_0(1710)) = (4.5 \pm 0.8) \cdot 10^{-3}$ or $Br(J/\psi \rightarrow \gamma f_0(1770)) = (3.7 \pm 0.8) \cdot 10^{-3}$ is found. This suggests a significant glueball component in this scalar state.

8 Acknowledgments

This work was done with the use of the IHEP (Protvino) Central Linux Cluster. The work is partially supported with the RFBR grant 20-02-00246.

References

- [1] Workman, R.L., *et al.*: Review of Particle Physics. PTEP **2022**, 083–01 (2022). <https://doi.org/10.1093/ptep/ptac097>
- [2] Bugg, D.V., *et al.*: Further amplitude analysis of $J/\psi \rightarrow \gamma(\pi^+\pi^-\pi^+\pi^-)$. Phys. Lett. B **353**, 378–384 (1995). [https://doi.org/10.1016/0370-2693\(95\)00525-P](https://doi.org/10.1016/0370-2693(95)00525-P)

- [3] Bai, J.Z., *et al.*: Partial wave analyses of $J/\psi \rightarrow \gamma K^+ K^-$ and $\gamma K^0(S) K^0(S)$. *Phys.Rev.D* **68**, 052003 (2003). <https://doi.org/10.1103/PhysRevD.68.052003>
- [4] Ablikim, M., *et al.*: Amplitude analysis of the $K_S K_S$ system produced in radiative J/ψ decays. *Phys. Rev D* **98**, 072003 (2018). <https://doi.org/10.1103/PhysRevD.98.072003>
- [5] Ablikim, M., *et al.*: Partial wave analyses of $J/\psi \rightarrow \gamma \pi^+ \pi^-$ and $\gamma \pi^0 \pi^0$. *Phys.Lett.B* **642**, 441–448 (2006). <https://doi.org/10.1016/j.physletb.2006.10.004>
- [6] Ablikim, M., *et al.*: Observation of a near-threshold enhancement in the $\omega\phi$ mass spectrum from the doubly OZI suppressed decay $J/\psi \rightarrow \gamma\omega\phi$. *Phys. Rev. Lett.* **96**, 162002 (2006) <https://arxiv.org/abs/hep-ex/0602031>. <https://doi.org/10.1103/PhysRevLett.96.162002>
- [7] Ablikim, M., *et al.*: Study of the near-threshold $\omega\phi$ mass enhancement in doubly OZI-suppressed $J/\psi \rightarrow \gamma\omega\phi$ decays. *Phys. Rev. D* **87**(3), 032008 (2013) <https://arxiv.org/abs/1211.5668> [hep-ex]. <https://doi.org/10.1103/PhysRevD.87.032008>
- [8] Ablikim, M., *et al.*: Pseudoscalar production at $\omega\omega$ threshold in $J/\psi \rightarrow \gamma\omega\omega$. *Phys. Rev. D* **73**, 112007 (2006) <https://arxiv.org/abs/hep-ex/0604045>. <https://doi.org/10.1103/PhysRevD.73.112007>
- [9] Guo, X.-D., Ke, H.-W., Zhao, M.-G., Tang, L., Li, X.-Q.: Revisiting the determining fraction of glueball component in f_0 mesons via radiative decays of J/ψ . *Chin.Phys. C* **45**(2), 023104 (2021) <https://arxiv.org/abs/2003.07116> [hep-ph]. <https://doi.org/10.1088/1674-1137/abccad>
- [10] Bugg, D.V.: Four sorts of mesons. *Phys. Rep.* **397**, 257 (2004)
- [11] Ablikim, M., *et al.*: Amplitude analysis of the $\pi^0\pi^0$ system produced in radiative J/ψ decays. *Phys. Rev. D* **92**(5), 052003 (2015)
- [12] Sarantsev, A.V., Denisenko, I., Thoma, U., Klempt, E.: Scalar isoscalar mesons and the scalar glueball from radiative J/ψ decays. *Phys. Lett. B* **816**, 136227 (2021) <https://arxiv.org/abs/2103.09680> [hep-ph]. <https://doi.org/10.1016/j.physletb.2021.136227>
- [13] Ivashin, A., *et al.*: Evidence for a scalar meson resonance in the $\pi^- p \rightarrow n\omega\phi$ reaction. *AIP Conf. Proc.* **1257**(1), 262–266 (2010). <https://doi.org/10.1063/1.3483329>
- [14] Amelin, D.V., *et al.*: Resonances in the $\omega\omega$ system. *Phys. Atom. Nucl.* **69**, 690–698 (2006). <https://doi.org/10.1134/S1063778806040132>

- [15] Bityukov, S.I., *et al.*: Observation of resonance with mass $M = 1814$ MeV, decaying into $\pi^-\eta\eta$. *Phys.Lett.B* **268**, 137–141 (1991). [https://doi.org/10.1016/0370-2693\(91\)90935-J](https://doi.org/10.1016/0370-2693(91)90935-J)
- [16] Kholodenko, M.S.: Particle identification with the Cherenkov detector in the VES experiment. *JINST* **15**(07), 07024 (2020). <https://doi.org/10.1088/1748-0221/15/07/C07024>
- [17] Dorofeev, V.A., *et al.*: A new electromagnetic calorimeter for the updated VES setup. *Instrum. Exp. Tech.* **59**(5), 658–665 (2016). <https://doi.org/10.1134/S0020441216040175>
- [18] Ivashin, A.V., Khokhlov, Y.A., Matveev, V.D.: Upgraded data acquisition system for the VES setup. Technical aspects. Preprint in Russian at <http://web.ihep.su/library/pubs/2010/ps/2010-10.pdf> (2010)
- [19] Ekimov, A.V., *et al.*: The VES detector control system. Preprint in Russian at <http://web.ihep.su/library/pubs/2013/ps/2013-2.pdf> (2013)
- [20] Hyams, B., *et al.*: t Dependence and Production Mechanisms of the ρ , f and g Resonances from $\pi^-p \rightarrow \pi^-\pi^+n$ at 17.2 GeV. *Phys. Lett. B* **51**, 272–278 (1974). [https://doi.org/10.1016/0370-2693\(74\)90290-1](https://doi.org/10.1016/0370-2693(74)90290-1)
- [21] N.N. Achasov, N.N., Shestakov, G.N.: $\pi\pi$ scattering S wave from the data on the reaction $\pi^-p \rightarrow \pi^0\pi^0n$. *Phys.Rev. D* **67**, 114018 (2003). <https://doi.org/10.1103/PhysRevD.67.114018>
- [22] Chung, S.U., Trueman, T.L.: Positivity conditions on the spin-density matrix: A simple parametrization. *Phys. Rev. D* **11**, 633 (1975). <https://doi.org/10.1103/PhysRevD.11.633>
- [23] Gottfried, K., Jackson, J.D.: On the Connection between Production Mechanism and Decay of Resonances at High Energies. *Nuovo Cimento* **33**, 309 (1964). <https://doi.org/10.1007/BF02750195>
- [24] Cohen-Tannoudji, G., Salin, P., Morel, A.: A Simple Formulation of High-Energy Exchange Models in Terms of Direct-Channel Amplitudes. *Nuovo Cimento A* **55**, 412–422 (1968). <https://doi.org/10.1007/BF02857563>
- [25] Zemach, C.: Three pion decays of unstable particles. *Phys. Rev.* **133**, 1201 (1964). <https://doi.org/10.1103/PhysRev.133.B1201>
- [26] Agostinelli, S., *et al.*: GEANT4—a simulation toolkit. *Nucl. Instrum. Meth. A* **506**, 250–303 (2003). [https://doi.org/10.1016/S0168-9002\(03\)01368-8](https://doi.org/10.1016/S0168-9002(03)01368-8)
- [27] Okubo, S.: Phi meson and unitary symmetry model. *Phys. Lett.* **5**, 165–168 (1963). [https://doi.org/10.1016/S0375-9601\(63\)92548-9](https://doi.org/10.1016/S0375-9601(63)92548-9)

- [28] Zweig, G.: An SU(3) model for strong interaction symmetry and its breaking I. CERN report TH-401 (1964)
- [29] Iizuka, J.: Systematics and phenomenology of meson family. Prog. Theor. Phys. Suppl. **38**, 21–34 (1966). <https://doi.org/10.1143/PTPS.37.21>
- [30] Nomokonov, V.P., Sapozhnikov, M.G.: Experimental tests of the Okubo-Zweig-Iizuka rule in hadron interactions. Phys.Part.Nucl. **34**, 94–123 (2003) <https://arxiv.org/abs/hep-ph/0204259>
- [31] Isgur, N., Thacker, H.B.: On the origin of the OZI rule in QCD. Phys. Rev. D **64**, 094507 (2001). <https://doi.org/10.1103/PhysRevD.64.094507>
- [32] Kolbig, K.S., Margolis, B.: Particle production in nuclei and unstable particle cross-sections. Nucl. Phys. B **6**, 85–101 (1968). [https://doi.org/10.1016/0550-3213\(68\)90271-X](https://doi.org/10.1016/0550-3213(68)90271-X)
- [33] Guisan, O., Bonamy, P., Le Du, P., Paul, L.: Study of $\pi^-p \rightarrow \pi^0n$ and $\pi^-p \rightarrow \eta n$ reactions in nuclei at 7.82 GeV/c. Nucl. Phys. B **32**, 681–690 (1971). [https://doi.org/10.1016/0550-3213\(71\)90500-1](https://doi.org/10.1016/0550-3213(71)90500-1)
- [34] Apokin, V.D., *et al.*: Determination of the cross-section of the process $\pi^+\pi^- \rightarrow \pi^0\pi^0$ in the dipion mass range $0.5 \text{ GeV} < M < 2 \text{ GeV}$ from the reaction $\pi^-p \rightarrow \pi^0\pi^0n$ at 39.1 GeV/c. Sov. J. Nucl. Phys. **49**, 278 (1989)
- [35] Chew, G.F., Low, F.E.: Unstable particles as targets in scattering experiments. Phys. Rev. **113**, 1640–1648 (1959). <https://doi.org/10.1103/PhysRev.113.1640>
- [36] Williams, P.K.: Extrapolation model for $\pi\pi$ scattering. Phys. Rev. D **1**, 1312–1318 (1970). <https://doi.org/10.1103/PhysRevD.1.1312>
- [37] Gui, L.-C., Chen, Y., Li, G., Liu, C., Liu, Y.-B., Ma, J.-P., Yang, Y.-B., Zhang, J.-B.: Scalar Glueball in Radiative J/ψ Decay on the Lattice. Phys. Rev. Lett. **110**(2), 021601 (2013) <https://arxiv.org/abs/1206.0125> [hep-lat]. <https://doi.org/10.1103/PhysRevLett.110.021601>
- [38] Close, F.E., Farrar, G.R., Li, Z.: Determining the gluonic content of isoscalar mesons. Phys. Rev. D **55**, 5749–5766 (1997) <https://arxiv.org/abs/hep-ph/9610280>. <https://doi.org/10.1103/PhysRevD.55.5749>